

Supporting Information

Glucose oxidase and conjugated polymers nanocomplexes for synergistic photothermal/starvation/oxidation therapy

Wei Zhang,^{*a} Wenhai Lin,^b Zhensheng Li,^c Tingting Sun^{*d} and Zhigang Xie^{*d}

^a *Tianjin Key Laboratory of Drug Targeting and Bioimaging, Life and Health Intelligent Research Institute, Tianjin University of Technology, Tianjin 300384, P. R. China*

^b *Biomedical Polymers Laboratory, College of Chemistry, Chemical Engineering and Materials Science, and State Key Laboratory of Radiation Medicine and Protection, Soochow University, Suzhou 215123, PR China*

^c *Key Laboratory of Chemo/Biosensing and Detection, College of Chemical and Materials Engineering, Xuchang University, Henan 461000, PR China*

^d *State Key Laboratory of Polymer Physics and Chemistry, Changchun Institute of Applied Chemistry, Chinese Academy of Sciences, 5625 Renmin Street, Changchun, Jilin 130022, P. R. China*

Contents

1. **Fig. S1** Synthetic route of imidazolyl substituted conjugated polymer IBDDP.
2. **Fig. S2** Corresponding ^1H NMR, ^{13}C NMR and mass spectrometry spectra of various BODIPY monomers.
3. **Fig. S3** Corresponding ^1H NMR of various IBDDP conjugated polymers.
4. **Fig. S4** (A) Representative images of different forms of nanocomplexes dispersions with different IBDDP/GOx ratios: 1/0, 1/3, 1/5, 2/1, 5/1, and 10/1. (B) Summary table of the diameter, PDI and zeta potential of different forms of NPs.
5. **Fig. S5** (A) Standard curve of IBDDP polymers determined by UV-vis absorption spectra. (B) Standard curve of BSA for the BCA protein assay kit.
6. **Fig. S6** Size and PDI changes of IBDDP&GOx NPs in (A) aqueous solution and (B) PBS with 10% FBS as a function of time measured by DLS.
7. **Fig. S7** Fluorescence spectra of IBDDP in CH_2Cl_2 , IBDDP conjugate polymer in THF, and IBDDP&GOx NPs in aqueous solution.
8. **Fig. S8** (A) Representative pictures of the working solution after treatment with GOx and IBDDP&GOx NPs. (B) The standard curve of H_2O_2 with different concentrations derived from the absorption of $\text{Ti(IV)O}_2\text{SO}_4$ at $\text{Abs}_{407\text{nm}}$. (C) UV-vis absorption spectra of formed Ti(IV)OSO_4 at different IBDDP&GOx NPs concentrations (GOx: 1-10 $\mu\text{g mL}^{-1}$, i-iv).
9. **Fig. S9** Photothermal response of (A) IBDDP&GOx NPs (50 $\mu\text{g mL}^{-1}$) and (B) IBDDP NPs (50 $\mu\text{g mL}^{-1}$) under corresponding irradiation (685 nm: 0.61 W cm^{-2}) and 5 min later the laser was shut down. Linear time data versus $-\ln\theta$ of (C) IBDDP&GOx NPs and (D) IBDDP NPs obtained from the cooling period.
10. **Fig. S10** PTT heating-up curves of IBDDP NPs at (A) different concentrations (5-50 $\mu\text{g mL}^{-1}$) and (B) laser power densities (0.38-1.05 W cm^{-2}) as a function of irradiation time. Heating reproducibility of (C) IBDDP NPs solution (50 $\mu\text{g mL}^{-1}$) over multiple laser on/off cycles under 685 nm (0.61 W cm^{-2}) laser irradiation. (D) Thermal images of IBDDP NPs (IBDDP: 50 $\mu\text{g mL}^{-1}$) solutions upon 685 nm laser irradiation at 0.61 W cm^{-2} at different times, respectively.
11. **Fig. S11** (A) FCM results of HeLa cells incubated with IBDDP&GOx NPs (IBDDP: 20 $\mu\text{g mL}^{-1}$) at 37 °C for 0.5, 2 and 4 h and at 4 °C for 0.5 h. (B) Quantitative analysis of endocytosis efficiency of IBDDP&GOx NPs by HeLa cells cotreated with different inhibitors (amiloride/genestein/glucose/ NaN_3) and IBDDP&GOx NPs for 4 h via FCM.

12. **Fig. S12** (a) Fluorescent images of PI (red, dead cells) and calcein-AM (green, live cells) co-stained HeLa cells incubated with IBDDP NPs (IBDDP: 35.5 $\mu\text{g mL}^{-1}$), GOx (GOx: 1.5 $\mu\text{g mL}^{-1}$) or IBDDP&GOx NPs (IBDDP: 35.5 $\mu\text{g mL}^{-1}$, GOx: 1.5 $\mu\text{g mL}^{-1}$) in the presence or absence of laser irradiation. Scale bar, 100 μm .

13. **Fig. S13** Typan blue stained HeLa cells after treatment with IBDDP NPs, GOx or IBDDP&GOx NPs after exposure to 685 nm laser irradiation, with blue color indicating dead cells. Scale bar, 100 μm .

14. **Fig. S14** Detection of mitochondrial potential changes in different groups (IBDDP NPs: IBDDP-35.5 $\mu\text{g mL}^{-1}$, GOx-1.5 $\mu\text{g mL}^{-1}$, IBDDP&GOx NPs: IBDDP-35.5 $\mu\text{g mL}^{-1}$, GOx-1.5 $\mu\text{g mL}^{-1}$) by JC-1 staining in the presence or absence of laser irradiation at 37 $^{\circ}\text{C}$. Scale bars, 100 μm .

15. **Fig. S15** Standard curve of ATP measured by an ATP assay kit.

16. **Fig. S16** Western blot analyses of Hsp90 expression in HeLa cells with different treatments after incubation for 1 h. The cells were treated with PBS, GOx, IBDDP NPs and IBDDP&GOx NPs with or without 658 nm laser irradiation (0.61 W cm^{-2} , 7 min).

Materials and Characterization: The starting materials 3,4-dihydroxybenzaldehyde was bought from Tianjin Xi'ensi Biochemical Technology Co., Ltd.. 1,6-Dibromohexane was purchased from Adamas Reagent Co., Ltd.. N-iodosuccinimide was purchased from Multipoint Chemical Reagent Co., Ltd.. 2,4-Dimethylpyrrole was bought from Suzhou Boke Chemical Co., Ltd.. 1-Methylimidazole, o-dianisidine, amiloride, genistein and GOx was bought from Thain Chemical Technology Co., Ltd.. 2,5-Bis(2-octyldodecyl)-3,6-bis(5-(4,4,5,5-tetramethyl-1,3,2-diborate-2-yl)thiophene-2-yl)[3,4-c]pyrrole-1,4(2H,5H)-dione (M1) was bought from Suzhou Nakai Technology Co., Ltd.. Horseradish peroxidase (≥ 300 u/mg), Annexin V-FITC apoptosis detection kits and Lyso Tracker Green were purchased from Shanghai Beyotime Biotechnology Co., Ltd.. Cell viability (live/dead cell staining) assay kit and Hoechst 33258 were purchased from Jiangsu KeyGEN Biotechnology Co., Ltd.. All reagents were purchased from commercial sources and used without further treatment, unless indicated otherwise.

^1H NMR spectra were measured in CDCl_3 and DMSO at room temperature by an AV-400 NMR spectrometer from Bruker. UV-vis and fluorescence spectra were recorded on SHIMADZU UV-2450 and Edinburgh Instrument FLS-920 spectrometers, respectively. The diameter and surface potential of the nanoparticles were determined by a Malvern Zetasizer Nano. The measurement was carried out at 25 °C, and the scattering angle was fixed at 90° . The morphology of the nanoparticles was measured by transmission electron microscopy (TEM) performed on a JEOL JEM-1011 electron microscope operating at an acceleration voltage of 100 kV. To prepare specimens for TEM, a drop of NPs solution (0.1 mg mL^{-1}) was deposited onto a copper grid with a carbon coating. The specimens were air-dried and measured at room temperature. Confocal laser scanning microscopy (CLSM) images were taken using a Zeiss LSM 700 (Zurich, Switzerland). Flow cytometry was carried out on Guava easyCyt 6-2L Base System (Merck Millipore, USA).

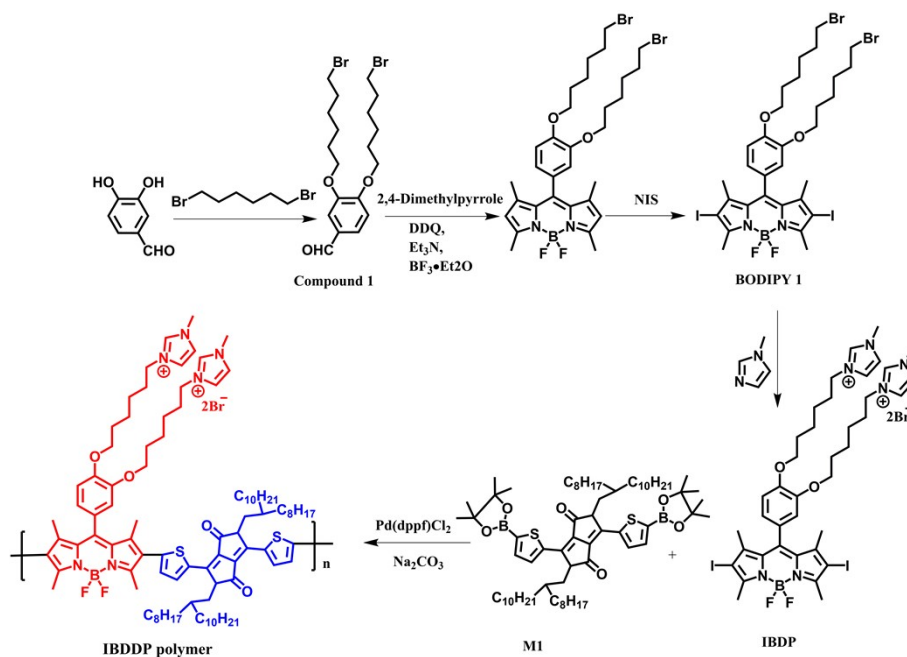


Fig. S1 Synthetic route of imidazolyl substituted conjugated polymer IBDDP.

Synthesis of Compound 1: 3,4-dihydroxybenzaldehyde (3.45 g, 25 mmol), 1,6-dibromohexane (61 g, $\times 10$ eqv.) were mixed with K_2CO_3 (13.8 g) and a catalytic amount of 18-crown-6 in 55 mL DMF, and then the mixture was heated to 80 °C in N_2 . After refluxing for 4 h, the reaction was cooled to R.T. and the solution was dried under vacuum. The mixture was extracted with brine and CH_2Cl_2 to obtain the crude product. After purification via a silica gel column, a yellowish oily liquid was obtained (ethyl acetate:petroleum ether=1:10). Yield: 63%, 1H NMR (400 MHz, $CDCl_3$) δ =9.38 (s, 1H), 7.49-7.33 (m, 2H), 6.95 (d, 1H), 4.07 (dt, 4H), 3.42 (t, 4H), 1.96-1.81 (m, 8H), 1.57-1.47 (m, 8H). ^{13}C NMR (400 MHz, $CDCl_3$) δ =156.62 (s), 149.83 (s), 145.40 (s), 141.44 (s), 131.63 (s), 126.80 (s), 120.38 (s), 113.25 (d, J =93.1 Hz), 33.23 (dd, J =114.3, 2.9 Hz), 28.48 (dd, J =111.6, 5.0 Hz), 25.24 (d, J =8.9 Hz), 16.57 (d, J =108.2 Hz).

Synthesis of BODIPY 1: NIS (1.4 g, 6.2 mmol) was added to the $CHCl_3$ solution of compound 1 (1.53 mmol) and then stirred at R.T. for 6 h. After the reaction was terminated, the mixture was extracted with CH_2Cl_2 and purified with a silica gel column (CH_2Cl_2 : hexane=1:1) to obtain a dark red solid powder. 1H NMR (400 MHz, $CDCl_3$) δ =6.98 (d, 1H), 6.80-6.67 (m, 2H), 4.07 (t, 2H), 3.95 (t, 2H), 3.43 (dt, 4H), 2.64 (s, 6H), 1.98-1.79 (m, 8H), 1.54 (s, 8H), 1.49 (s, 6H). ^{13}C NMR (400 MHz, $CDCl_3$) δ =191.02 (s), 154.48 (s), 149.28 (s), 129.40 (d, J =103.1 Hz), 126.75 (s), 111.23 (d, J =94.9 Hz), 68.79 (s), 53.10 (d, J =80.3 Hz), 33.81 (t, J =2.9 Hz), 32.59 (dd, J =16.4, 5.4 Hz), 29.04-28.29 (m), 27.87 (d, J =4.6 Hz), 25.28 (dd, J =12.6, 4.4 Hz).

Synthesis of imidazolyl-substituted IBDP: BODIPY 1 (100 mg, 0.11 mmol) and 1-methylimidazole (0.2 mL) were dissolved in 15 mL acetonitrile and then heated and refluxed at 85 °C overnight. Furthermore, the organic solvent was drained out, and the remaining substance was repeatedly recrystallized in ethanol to obtain the final red solid with a yield of 94%. ¹H NMR (400 MHz, DMSO) δ=9.14 (d, 2H), 7.78 (d, 2H), 7.71 (d, 2H), 7.13 (d, 1H), 6.98 (d, 1H), 6.87 (dd, 1H), 4.16 (dt, 4H), 3.99 (dt, 4H), 3.85 (d, 6H), 3.33 (s, 6H), 2.54 (t, 6H), 1.76 (ddd, 8H), 1.48-1.39 (m, 8H). ¹³C NMR (400 MHz, DMSO) δ=158.65 (s), 136.84 (s), 123.83 (s), 122.72 (s), 117.54 (s), 116.00-110.54 (m), 68.71 (d, J=30.7 Hz), 60.21 (s), 49.15 (s), 36.20 (s), 28.80 (d, J=13.0 Hz), 25.45 (dd, J=46.2, 6.5 Hz), 16.27-11.61 (m).

Synthesis of conjugated polymer IBDDP: IBDP (76 mg, 0.10 mmol), M1 (111 mg, 0.10 mmol), Pd(dppf)Cl₂ (13 mg) and Na₂CO₃ (106 mg, 1.00 mmol) were placed in a 250 mL round-bottomed flask with support, and the tube was evacuated and back-filled with argon three times. A degassed solvent mixture of toluene (16 mL), ethanol (8 mL) and water (3 mL) was transferred to the round-bottomed flask through a septum, and the reaction mixture was purged with argon for 15 min. The reaction was carried out at 85 °C for 12 h under an argon atmosphere, and the reaction was continued for 24 h. After completion, the solvent was removed under reduced pressure, the mixture was dissolved in 10 mL of CHCl₃, and the solution was poured slowly into 250 mL of cold methanol under vigorous stirring. After 15 min of stirring, the polymer was collected by vacuum filtration, and the above process was repeated several times. ¹H NMR (400 MHz, CDCl₃) δ=8.94(s, 2H), 7.63-7.37(m, 8H), 6.98(s, 1H), 6.86(s, 2H), 5.34(s, 2H), 5.00(s, 2H), 4.69(s, 2H), 4.28(s, 4H), 4.00(d, 7H), 2.65(s, 4H), 2.22(d, 4H), 1.90(d, 7H), 1.40(d, 6H), 1.23(d, 62H), 0.84(s, 17H).

Preparation of IBDDP@GOx NPs: The nanocomplexes were mainly prepared by the ultrasonic emulsification method with different feeding ratios of IBDDP and GOx (1/0, 1/3, 1/5, 2/1, 5/1 and 10/1). Briefly, IBDDP was dissolved in 2 mL THF and then slowly dropped into GOx aqueous solution (10 mL) under high-power ultrasound, and subsequently, the mixture was quickly shaken until the THF completely evaporated to obtain the IBDDP@GOx NPs. After that, the obtained nanoparticles were stirred for another 4 h at R.T. continuously for the sake of removing the possible remaining organic reagents. The concentrations of IBDDP and GOx were determined by UV-vis absorption spectroscopy and BCA protein content determination kits,

respectively. Furthermore, NPs with an IBDDPP/GOx mass ratio of 1/0 were used as the control.

Photothermal performance: IBDDP@GOx NPs solutions with different concentrations ($5\text{--}50\ \mu\text{g mL}^{-1}$) were irradiated with a 685 nm laser ($0.61\ \text{W cm}^{-2}$, 5 min) or different powers ($0.38\text{--}1.05\ \text{W cm}^{-2}$) at a fixed concentration. The temperatures were recorded every 10 s. The photothermal response of IBDDP@GOx NPs ($25.0\ \mu\text{g mL}^{-1}$, 200 μL) was recorded with laser irradiation ($685\ \text{nm}$, $0.61\ \text{W cm}^{-2}$, 5 min) and then shut off, and temperatures were also recorded every 10 s. The cycling heating-cooling curves were investigated by determining their absorbance changes upon continuous 685 nm laser irradiation ($0.61\ \text{W cm}^{-2}$) and temperatures were recorded every 10 s. The temperature change images were taken by a near-infrared thermal camera. The photothermal conversion efficiency (η) was calculated according to formulas reported in other literature¹.

Glucose oxidase activity detection: The enzyme activity of GOx was evaluated by cascade reaction with horseradish peroxidase (HRP) and *o*-dianisidine². It was mainly to monitor the change in oxidized *o*-dianisidine at 460 nm measured by UV-vis spectroscopy, while obvious color changes could be observed for detecting the working solution with the naked eye. Working solution: *o*-dianisidine (2.5 mL, 0.33 mM), 18% glucose (0.3 mL), 0.02% HRP (0.1 mL). All solutions mentioned above were prepared with 0.1 M PBS (pH 6.0) buffer. Since *o*-dianisidine was insoluble in H₂O, it could be dissolved with a small amount of MeOH and then diluted with PBS buffer. 0.1 mL IBDDP&GOx NPs solution or GOx solution was quickly added to the above working solution, and the change in absorbance at 460 nm over different time periods was recorded. The initial slope of the curve was used to evaluate the activity of GOx.

H₂O₂ generation detection: To further determine the catalytic capability of GOx of IBDDP&GOx NPs, titanium oxysulfate (Ti(IV)OSO₄) detection was carried out. H₂O₂ generated via glucose degradation catalyzed by GOx could oxidize Ti(IV)OSO₄ to form a yellow peroxidized complex Ti(IV)O₂SO₄, which exhibited an obvious characteristic UV absorption peak at 407 nm³. Working solution: acetone (500 μL), Ti(IV)OSO₄ (50 μL , 30 mM), NH₃•H₂O (100 μL) and H₂SO₄ solution (500 μL , 1 M). The experimental process was as follows: various concentrations of IBDDP&GOx NPs were mixed with 10 mL glucose ($100\ \mu\text{g mL}^{-1}$), and then 100 μL solution was removed at different time points and quickly mixed with the above working solution.

Finally, the absorbance of all the solutions at 407 nm was measured, and the concentration of H₂O₂ was determined according to the fitting standard curve.

Cell lines and cell culture: Human cervical carcinoma (HeLa) cells were purchased from the Institute of Biochemistry and Cell Biology, Chinese Academy of Sciences, Shanghai, China. All the cells were grown in Dulbecco's modified Eagle's medium (DMEM, GIBCO) supplemented with 10% heat-inactivated fetal bovine serum (FBS, GIBCO), 100 U/mL penicillin and 100 µg mL⁻¹ streptomycin (Sigma), and the culture medium was replaced once every day. All the cells were cultured in a humidified incubator at 37 °C with 5% CO₂.

Cell endocytosis by confocal laser scanning microscopy (CLSM) and flow cytometry:

Cellular uptake of HeLa cells was examined by using a confocal laser scanning microscope (CLSM). HeLa cells were seeded in 6-well culture plates at a density of 5×10⁴ cells per well and allowed to adhere for 24 h. After that, the cells were treated with IBDDP&GOx NPs (IBDDP: 20.0 µg mL⁻¹) in complete DMEM for different time periods at 37 °C and at 4 °C. After that, the supernatant was carefully removed, and the cells were washed three times with PBS. Subsequently, the cells were fixed with 1 mL of 4% formaldehyde in each well for 10 min at room temperature and washed twice with PBS again. Then, the cell nuclei were stained with Hoechst 33258. The slides were mounted and observed with confocal laser scanning microscopy (Zeiss LSM 780). To determine the time-dependent cellular internalization of the nanoparticles, flow cytometry was carried out, which collected 5,000 cells per sample. Cells were seeded in 6-well plates at a density of 500,000 cells per well in 1.5 mL of medium and cultured for 24 h. The medium was replaced with IBDDP&GOx NPs (IBDDP: 20.0 µg mL⁻¹). After incubation at 37 °C for 4 h, 2 h and 0.5 h and at 4 °C for 0.5 h, the cells were washed with PBS and treated with trypsin. The harvested cells were suspended in PBS and centrifuged at 2000 rpm for 5 min. The supernatants were discarded, and the cells were washed again with PBS to remove the medium. After washing, the cells were resuspended in 500 µL PBS before analysis by Guava easyCyte 6-2L Base System (Merck Millipore, USA). To determine the specific endocytosis pathway of IBDDP&GOx NPs by FCM, the basic experimental process was the same as the above method. The only difference was pretreatment of HeLa cells with various endocytosis pathway inhibitors (amiloride: 13 µg mL⁻¹, sucrose: 154 µg mL⁻¹, genistein: 27 µg mL⁻¹, NaN₃: 1 mg mL⁻¹).

Cellular ROS generation of IBDDP&GOx NPs: A commercial ROS detection kit

was used to detect the H₂O₂ generated from the catalytic reaction of glucose in the presence of IBDDP&GOx NPs. HeLa cells were seeded into 6-well culture plates with a sterile cover slip. After 24 h, normal DMEM was removed, and the tumor cells were thoroughly washed with PBS three times. Subsequently, IBDDP&GOx NPs, IBDDP NPs and GOx in low-glucose DMEM were added for further incubation at 37 °C for another 2 h. Then, HeLa cells were washed with PBS three times, and DCFH-DA detection working solution was added to each well for 30 min. After that, the cells were washed with serum-free DMEM and imaged with CLSM without fixation.

Cytotoxicity assays: To evaluate the in vitro cytotoxicity of IBDDP&GOx NPs, we measured the cell viabilities via MTT assays. The absorbance of the formazan product was measured at 490 nm with a Bio-Rad 680 microplate reader. Cell viability (%) was calculated by the following equation: $(A_{\text{sample}}/A_{\text{control}}) \times 100\%$, where A_{sample} and A_{control} are the absorbances of the sample well and control well, respectively.

First, the cytotoxicity of IBDDP&GOx NPs, IBDDP NPs and GOx in normal DMEM (4.5 g/L) was characterized. HeLa cells with a density of 1×10^4 were plated in 96-well plates and incubated for 24 h to fully adhere to the plate. Next, the medium was replaced with different NPs at various concentrations. IBDDP&GOx NPs (GOx: 0.1875, 0.375, 0.75, 1, 1.5 $\mu\text{g mL}^{-1}$; IBDDP: 4.4375, 8.875, 17.75, 23.7, 36.5 $\mu\text{g mL}^{-1}$), IBDDP NPs (IBDDP: 4.4375, 8.875, 17.75, 23.7, 36.5 $\mu\text{g mL}^{-1}$) and GOx (0.1875, 0.375, 0.75, 1, 1.5 $\mu\text{g mL}^{-1}$). Furthermore, we further investigated the cellular toxicity of GOx on HeLa cells in glucose-free DMEM. Before the MTT experiment, HeLa cells were thoroughly centrifuged with PBS 3 times and then redispersed in glucose-free DMEM. Next, different concentrations of GOx (10, 5, 2, 1, 0.5, 0.05 $\mu\text{g mL}^{-1}$) in glucose-free DMEM were added to the plate and cultured continuously for 24 h. In addition, the effects of glucose (2, 1, 0.5, 0.25, 0.1, 0.05 mg mL^{-1}) and H₂O₂ (2, 1, 0.5, 0.25, 0.1, 0.05 mM) in normal DMEM on HeLa cell proliferation were also evaluated by MTT assays. Finally, to comprehensively evaluate the synergistic photothermal/starvation/oxidation therapy effect of IBDDP&GOx NPs on HeLa cells, different concentrations of IBDDP&GOx NPs (GOx: 0.1875, 0.375, 0.75, 1, 1.5 $\mu\text{g mL}^{-1}$; IBDDP: 4.4375, 8.875, 17.75, 23.7, 36.5 $\mu\text{g mL}^{-1}$), IBDDP NPs (IBDDP: 4.4375, 8.875, 17.75, 23.7, 36.5 $\mu\text{g mL}^{-1}$) or GOx (0.1875, 0.375, 0.75, 1, 1.5 $\mu\text{g mL}^{-1}$) in low-glucose DMEM (1 g/L) were added to the incubation system. After incubation for 6 h, all the experimental groups were irradiated with a 685 nm laser (0.61 W cm^{-2} , 7 min). After irradiation and temperature

cooling, all the above medium was removed and replaced with new medium. The cell viability was determined by MTT colorimetry after 24 h and calculated as described above.

Live/dead cell staining assays: To further confirm the synergistic photothermal/starvation/oxidation therapy efficacy of IBDDP&GOx NPs, HeLa cells were stained with calcein-AM/propidium iodide (PI) to determine their viabilities. Briefly, the cells were incubated with IBDDP&GOx NPs (GOx: 1.5 $\mu\text{g mL}^{-1}$; IBDDP: 36.5 $\mu\text{g mL}^{-1}$), IBDDP NPs (IBDDP: 36.5 $\mu\text{g mL}^{-1}$) and GOx (1.5 $\mu\text{g mL}^{-1}$) in low-glucose DMEM (1 g/L) for 6 h and then irradiated with a 685 nm laser at 0.61 W cm^{-2} for 7 min. The cells treated without laser irradiation were set as the controls at the same time. After that, the cells were further incubated at 37 °C for an additional 24 h. The cells were stained with calcein-AM (green for living cells) and PI (red for dead cells) for 30 min at room temperature. Subsequently, the cells were washed with PBS and finally imaged by a Nikon C1si laser scanning confocal microscope.

Trypan blue staining was also carried out to further demonstrate the cellular membrane integrity. In this process, living cells would not be stained, while dead cells would appear light blue. The experimental process was almost the same as the above procedures. After incubation for 24 h, the tumor cells were treated with trypsin and diluted to prepare a single cellular suspension. Subsequently, the cell suspension was mixed with 0.4% trypan blue solution at 9:1. The cells were observed under optical microscopy. The dead cells were dyed obviously blue, while the living cells were colorless and transparent.

Determination of ATP content in cells:

To verify that the ATP expression of tumor cells would be affected by the constant consumption of glucose by IBDDP&GOx NPs, we evaluated the intracellular ATP level of different experimental groups. We first prepared a cellular suspension of HeLa cells in low-glucose DMEM and inoculated it into a 6-well cell culture plate at a density of 5×10^4 cells/well. After 24 h, the cells were incubated with IBDDP&GOx NPs (GOx: 1 $\mu\text{g mL}^{-1}$; IBDDP: 23.7 $\mu\text{g mL}^{-1}$) and IBDDP NPs (IBDDP: 23.7 $\mu\text{g mL}^{-1}$) for 6 h and 4 h. Subsequently, the cells were washed with PBS 3 times, and then the cells were collected and ensured to have the same number of cells for each sample. Finally, the obtained cells were lysed, and ATP expression was evaluated by an ATP chemiluminescence assay kit.

Immunofluorescence staining: To determine the expression of HSP90 in HeLa cells

under different treatments, immunofluorescence staining was utilized. The specific experimental procedures were as follows: (1) Sterile cover glasses (24×24 mm) were placed in a 6-well culture plate and sterilized with UV light for more than 30 min. (2) HeLa cells with a density of 1×10^4 were plated in a 6-well plate and incubated for another 24 h. (3) The medium was replaced with 1 mL IBDDP&GOx NPs (GOx: $1.5 \mu\text{g mL}^{-1}$, IBDDP: $36.5 \mu\text{g mL}^{-1}$), IBDDP NPs (IBDDP: $36.5 \mu\text{g mL}^{-1}$) and GOx (GOx: $1.5 \mu\text{g mL}^{-1}$) in low-sugar DMEM. (4) After incubation at 37 °C for 6 h, each one of the control, IBDDP&GOx NPs and IBDDP NPs group were irradiated with a 685 nm laser for 7 min at 0.61 W cm^{-2} . (5) After 1 h, anti-HSP90 antibody (1: 200) was added and further incubated at 4 °C overnight. (6) After washing with TBST solution, the HeLa cells were further labeled with Alexa Fluor 488-labeled goat anti-mouse IgG (H+L) (1:500) at R.T. for 2 h. (7) After staining with $10 \mu\text{g mL}^{-1}$ DAPI solution for 5 min at R.T., all the samples were observed with CLSM. DAPI and Alexa Fluor 488 were excited at 405 nm and 488 nm, respectively.

Western blot assays: To measure the expression level of HSP90. HeLa cells were planted in 6-well culture plates (1×10^6 cells per well, 1 mL of DMEM medium). The experiments were divided into 8 groups: (1) Control-37 °C; (2) Control-45 °C; (3) IBDDP NPs-37 °C; (4) IBDDP NPs-45 °C; (6) GOx-37 °C; (7) GOx-45 °C; (8) IBDDP&GOx NPs-37 °C; (9) IBDDP&GOx NPs-45 °C. Then, the cells were then collected using trypsin and lysed in lysis buffer. BCA protein assay was conducted to detect the protein content. Then, the proteins were separated by sodium dodecyl sulfate-polyacrylamide gel electrophoresis (SDS-PAGE) and moved to a polyvinylidene fluoride (PVDF) membrane. After 1 h blocking step with 5% dried skimmed milk, the membrane was cultivated with the corresponding primary antibody overnight on a shaker (4°C), followed by cultivation with the secondary antibody (1h, R.T.). Afterwards, the membrane was visualized by an ECLplus detection system.

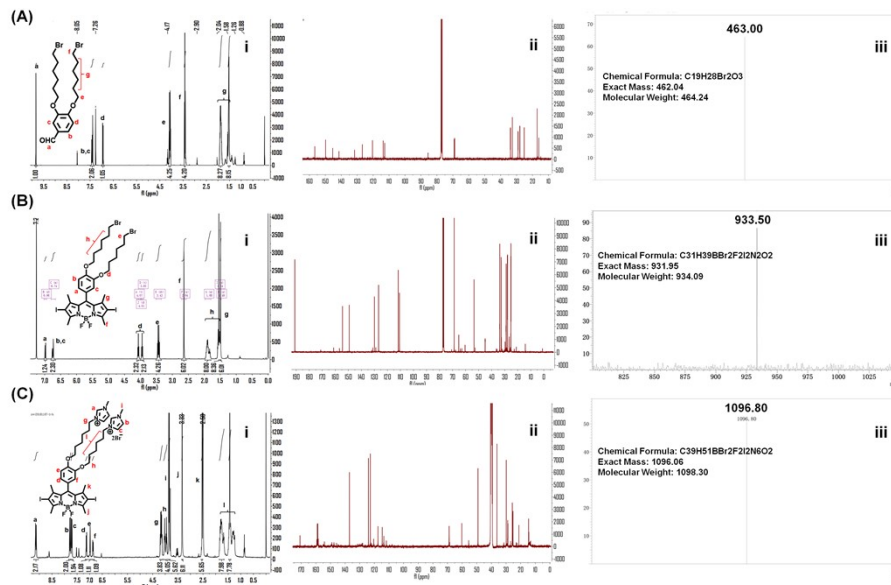


Fig. S2 Corresponding ^1H NMR, ^{13}C NMR and mass spectrometry spectra of various BODIPY monomers.

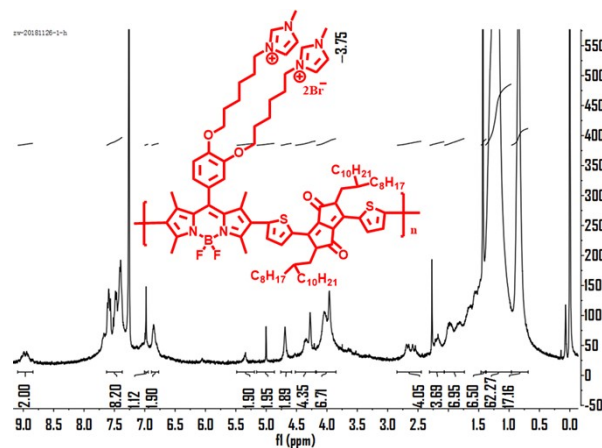


Fig. S3 Corresponding ^1H NMR of various IBDDP conjugated polymers.

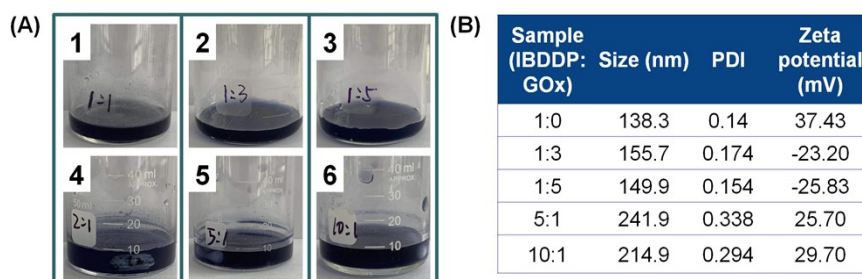


Fig. S4 (A) Representative images of different forms of nanocomplexes dispersions with different IBDDP/GOx ratios: 1/0, 1/3, 1/5, 2/1, 5/1, and 10/1. (B) Summary table of the diameter, PDI and zeta potential of different forms of NPs.

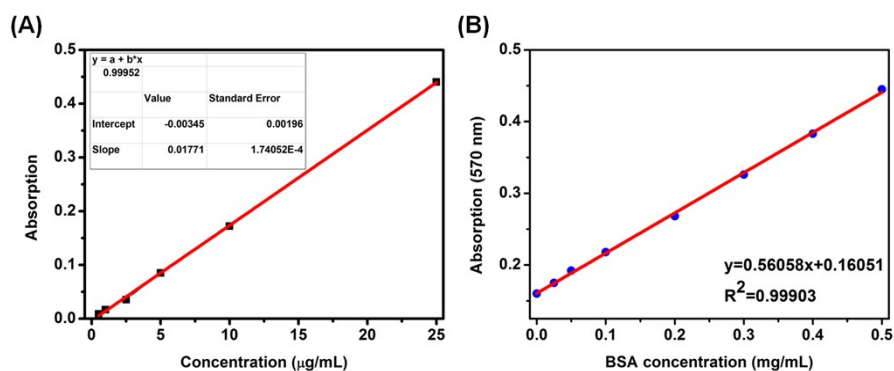


Fig. S5 (A) Standard curve of IBDDP polymers determined by absorption spectra. (B) Standard curve of BSA for the BCA protein assay kit.

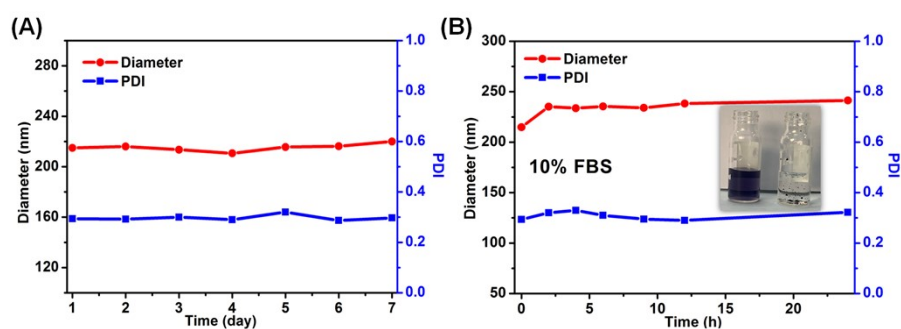


Fig. S6 Size and PDI changes of IBDDP&GOx NPs in (A) aqueous solution and (B) PBS with 10% FBS as a function of time measured by DLS.

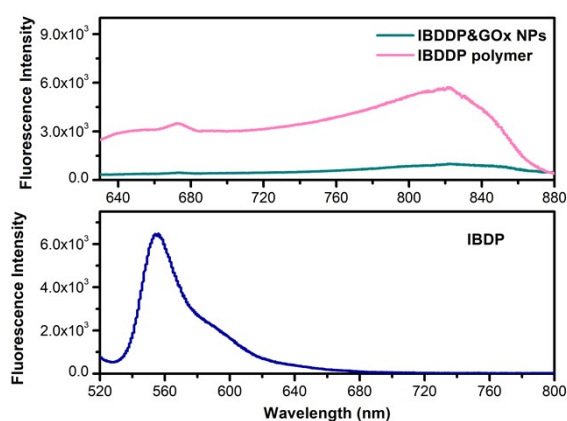


Fig. S7 Fluorescence spectra of IBDDP in CH_2Cl_2 , IBDDP conjugate polymer in THF, and IBDDP&GOx NPs in aqueous solution.

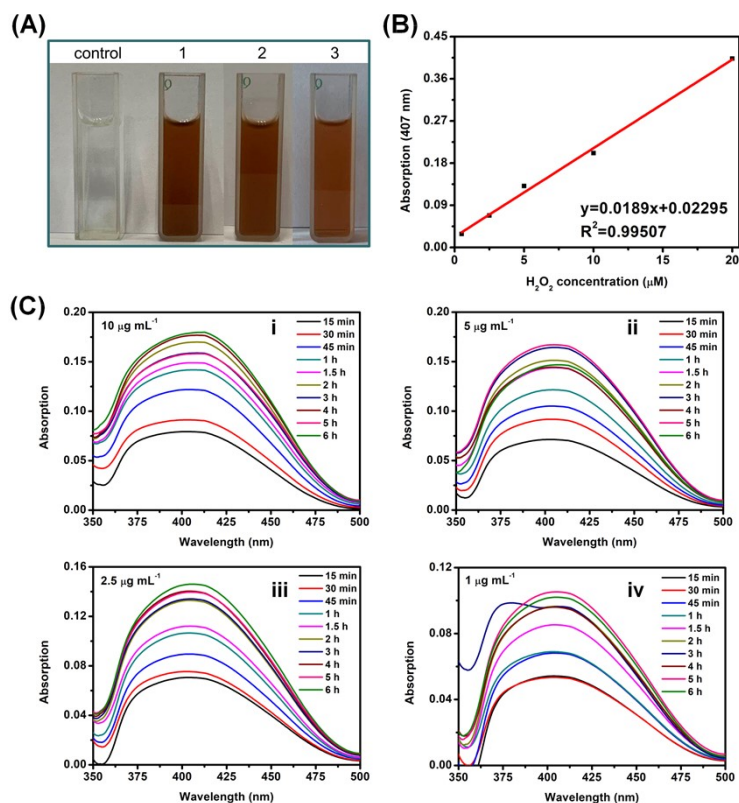


Fig. S8 (A) Representative pictures of the working solution after treatment with GOx and IBDDP&GOx NPs. (B) The standard curve of H₂O₂ with different concentrations derived from the absorption of Ti(IV)O₂SO₄ at 407nm. (C) UV-vis absorption spectra of formed Ti(IV)OSO₄ at different IBDDP&GOx NPs concentrations (GOx: 1-10 μg mL⁻¹, i-iv).

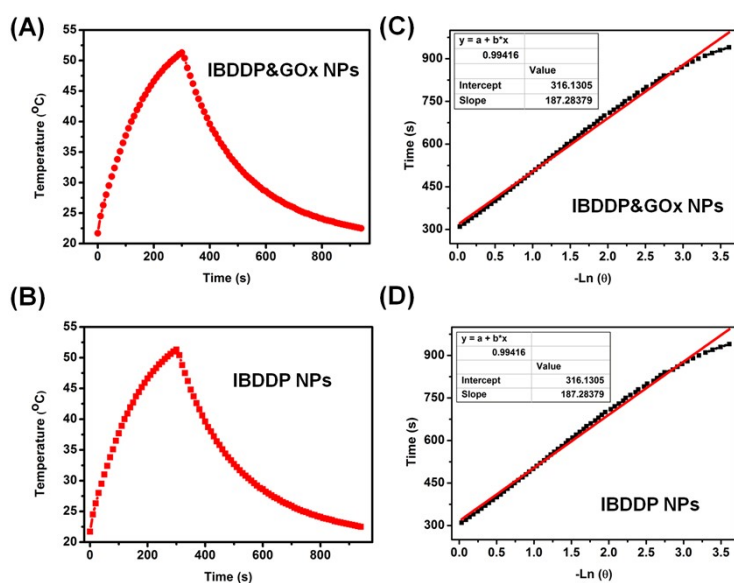


Fig. S9 Photothermal response of (A) IBDDP&GOx NPs (50 μg mL⁻¹) and (B)

IBDDP NPs ($50 \mu\text{g mL}^{-1}$) under corresponding irradiation (685 nm : 0.61 W cm^{-2}) and 5 min later the laser was shut down. Linear time data versus $-\ln\theta$ of (C) IBDDP&GOx NPs and (D) IBDDP NPs obtained from the cooling period.

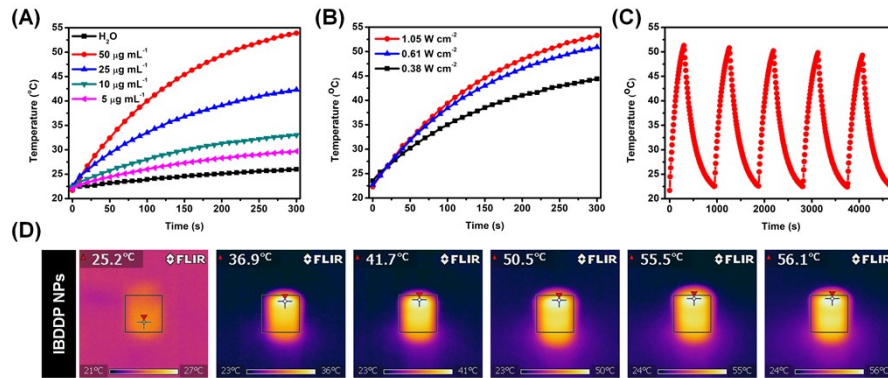


Fig. S10 PTT heating-up curves of IBDDP NPs at (A) different concentrations (5 – $50 \mu\text{g mL}^{-1}$) and (B) laser power densities (0.38 – 1.05 W cm^{-2}) as a function of irradiation time. Heating reproducibility of (C) IBDDP NPs solution ($50 \mu\text{g mL}^{-1}$) over multiple laser on/off cycles under 685 nm (0.61 W cm^{-2}) laser irradiation. (D) Thermal images of IBDDP NPs (IBDDP: $50 \mu\text{g mL}^{-1}$) solutions upon 685 nm laser irradiation at 0.61 W cm^{-2} at different times, respectively.

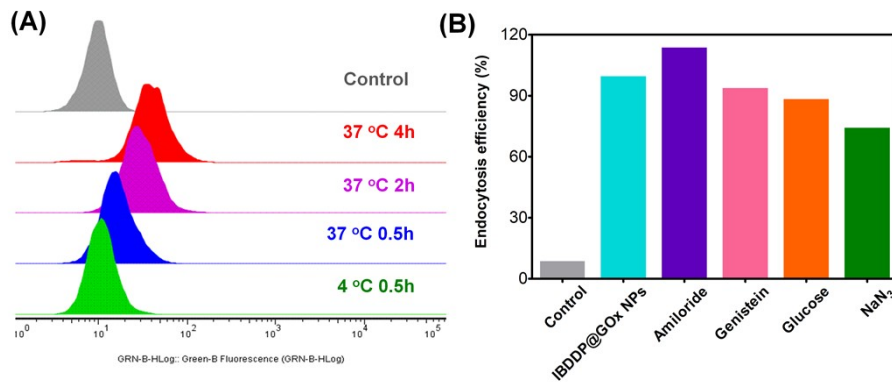


Fig. S11 (A) FCM results of HeLa cells incubated with IBDDP&GOx NPs (IBDDP: $20 \mu\text{g mL}^{-1}$) at $37 \text{ }^\circ\text{C}$ for 0.5 , 2 and 4 h and at $4 \text{ }^\circ\text{C}$ for 0.5 h . (B) Quantitative analysis of endocytosis efficiency of IBDDP&GOx NPs by HeLa cells cotreated with different inhibitors (amiloride/genestein/glucose/ NaN_3) and IBDDP&GOx NPs for 4 h via FCM.

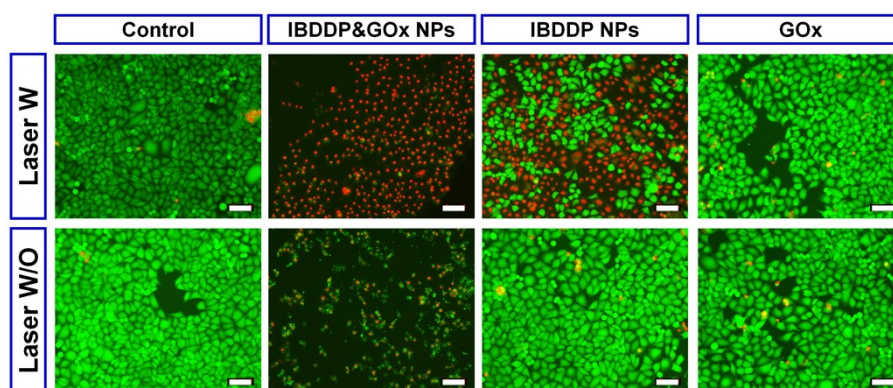


Fig. S12 (a) Fluorescent images of PI (red, dead cells) and calcein-AM (green, live cells) co-stained HeLa cells incubated with IBDDP NPs (IBDDP: $35.5 \mu\text{g mL}^{-1}$), GOx (GOx: $1.5 \mu\text{g mL}^{-1}$) or IBDDP&GOx NPs (IBDDP: $35.5 \mu\text{g mL}^{-1}$, GOx: $1.5 \mu\text{g mL}^{-1}$) in the presence or absence of laser irradiation. Scale bar, $100 \mu\text{m}$.

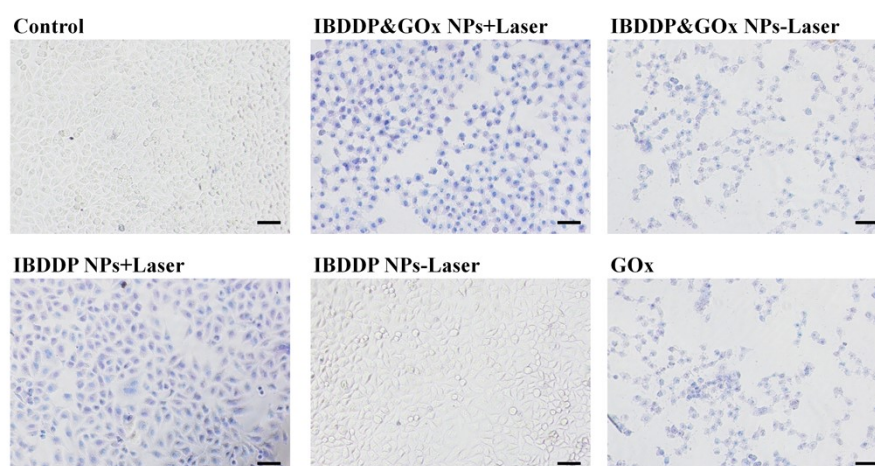


Fig. S13 Typan blue stained HeLa cells after treatment with IBDDP NPs, GOx or IBDDP&GOx NPs after exposure to 685 nm laser irradiation. Blue color indicates dead cells. Scale bar, $100 \mu\text{m}$.

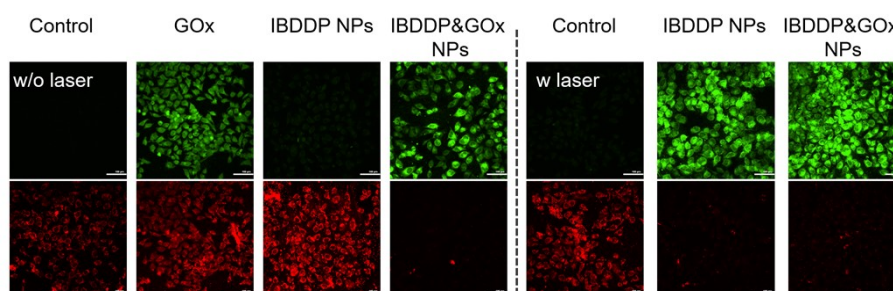


Fig. S14 Detection of mitochondrial potential changes in different groups (IBDDP NPs: IBDDP- $35.5 \mu\text{g/mL}$, IBDDP&GOx NPs: IBDDP- $35.5 \mu\text{g/mL}$, GOx- $1.5 \mu\text{g/mL}$)

by JC-1 staining in the presence or absence of laser irradiation at 37 °C. Scale bars, 100 μm .

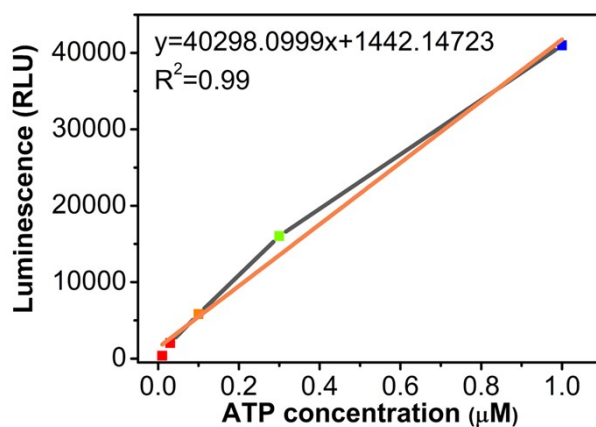


Fig. S15 Standard curve of ATP measured by an ATP assay kit.

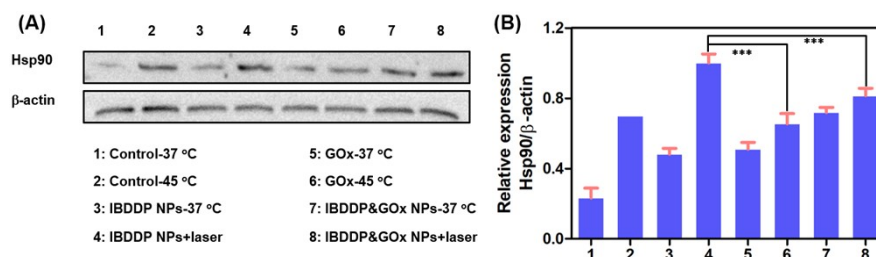


Fig. S16 Western blot analysis of HSP90 expression in HeLa cells with different treatments after incubation for 1 h. The cells were treated with PBS, GOx, IBDDP NPs or IBDDP&GOx NPs with or without 658 nm laser irradiation (0.61 W/cm², 7 min).

References:

1. Liu, Y.; Ai, K.; Liu, J.; Deng, M.; He, Y.; Lu, L., *Adv. Mater.* 33, 25 (9), 1353-1359.
2. Li, D.; He, Q.; Cui, Y.; Duan, L.; Li, J., *Biochem. Biophys. Res. Co.* 29, 355 (2), 488-493.
3. Fan, W.; Lu, N.; Huang, P.; Liu, Y.; Yang, Z.; Wang, S.; Yu, G.; Liu, Y.; Hu, J.; He, Q., *Angew. Chem.* 32, 129 (5), 1249-1253.